A narrow-linewidth Brillouin laser for a two-photon rubidium frequency standard

Kyle W. Martin[1], River Beard[1], Andrei Isichenko[2], Kaikai Liu[2], Seth E. Erickson[3], Kaleb Campbell[3], Daniel J. Blumenthal[2], Sean Krzyzewski[3*]

[1]AV Incorporated, 1300 Britt Street, Albuquerque, 87123, NM, USA.
[2]Department of Electrical and Computer Engineering, University of California, Santa Barbara, 93106, CA, USA.
[3*]Space Vehicles Directorate, Air Force Research Laboratory, Kirtland Air Force Base, 87117, NM, USA.

*Corresponding author(s). E-mail(s): qst@afrl.af.mil;

Abstract

High precision portable and deployable frequency standards are required for modern navigation and communication technologies. Optical frequency standards are attractive for their improved stability over their microwave counterparts; however, increased complexities have anchored them in the laboratory. Sacrificing sensitivity of the most stable optical clocks has led to the recent development of deployable and portable optical frequency standards, leveraging hot atomic or molecular vapor. The short term limit for a majority of previous reports on two-photon rubidium standards is either the shot-noise or intermodulation limit hindering the one second fractional frequency stability to around $1 \times 10^{-13}/\sqrt{\tau}$. The answer for the shot-noise limit is to increase optical power and collected fluorescence, while the intermodulation limit solution requires improvements in laser linewidth, stimulated Brillouin scattering (SBS) lasers are known to reduce frequency noise, suppressing noise of the pump laser at high ofset frequencies. We investigate an optical frequency standard based on the two-photon transition in ^{87}Rb probed with a narrow linewidth photonic integrated circuit SBS laser with a quality factor over 130 million and instantaneous linewidth < 10 Hz. The use of a narrow linewidth clock laser coupled with operating at higher optical intensities yields clock instabilities of 2×10^{-14} at one second, currently the best reported short-term stability for a two-photon rubidium optical frequency standard.

1 Introduction

Modern communication, navigation, and sensing systems rely on portable clocks and oscillators to provide necessary stable frequency and phase sources [1]. While crystal and MEMS oscillators meet a vast majority of timing needs, more precise and robust applications require atomic clocks. Microwave clocks based on rubidium and cesium are currently the most popular technology fulfilling this need [1, 2]. These atomic microwave standards have provided robust and stable phase and frequency sources and have well understood frequency shifts and drifts [3]. Nonetheless, emerging technologies such as femtosecond two-way optical time transfer [4–9] and high frequency distributed antenna systems [10, 11] require even more stable low size, weight, and power (SWaP) frequency standards. These emerging technologies coupled with improvements in existing communication, navigation, and sensing technologies adds significant value to portable atomic frequency standards with superior timing stability.

Current state-of-the-art single ion [12–14] and optical lattice clocks [15–17] yield excellent results in controlled laboratory environments. Efforts to bring these more advanced optical lattice and ion clocks from a laboratory environment into the field is an active area of research [18–23]. However, single ion and optical lattice clocks have yet to make an impact with more stringent requirements of SWaP, robustness, and autonomy necessary for widespread communication, navigation and sensing. Selective tradeoffs need to be made for advanced deployable clocks to be used in a more widespread manner.

In order to meet the stringent demands for deployable clocks, research teams have often elected to simplify the state-of-the-art optical clocks to prioritize certain advancements in frequency stabilization. Several efforts have maintained a fundamental microwave clock frequency while adding lasers for state preparation [24] or for laser cooling to reduce Doppler and collisional shifts [25]. Nevertheless, these microwave standards still lack the higher short term stability of their optical counterparts. Portable optical cavities have also garnered interest in recent years [26, 27]; while generally superior in performance at short-time scales, they lack an atomic reference and suffer from long-term frequency drifts. The use of hot atomic [28] or molecular vapors [29] have had recent success operating outside the laboratory in a relevant SWaP envelope. These hot atomic or molecular optical clocks retain high stability at short timescales (leveraging stable optical oscillators) while simultaneously benefiting from long-term stability of the probed atomic or molecular energy transitions.

We investigate the optical rubidium atomic frequency standard leveraging the $5S_{1/2}(F = 2) \rightarrow 5D_{5/2}(F = 4)$ transition in ^{87} Rb and detecting fluorescence decay along the $6P_{3/2} \rightarrow 5S_{1/2}$ [30–41]. This transition has several advantages as the required clock laser can be generated through second harmonic generation of telecom C-band laser systems, the fluorescence is easy to distinguish from the clock laser at 778 nm, as well as the relatively high excitation rate for a two-photon system. However, the short term clock performance is generally limited by either photon shot-noise or laser frequency noise in the form of intermodulation limit [31]. In this article, we demonstrate an order-of-magnitude improvement on both of the short-term limitations by using high intensity to suppress photon shot-noise and a photonic integrated silicon nitride stimulated Brillouin scattering (SBS) laser to reduce the intermodulation limit.

2 Short-term clock limits

A recent review article of the $5S_{1/2} \rightarrow 5D_{5/2}$ two-photon transition in Rb [31] concluded that for the majority of reports the short-term limit is either the photon shot-noise or laser frequency noise in the form the the intermodulation limit.

2.0.1 Photon Shot-Noise Limit

The statistical uncertainty involved in detecting photons gives rise to a fundamental limitation to any photo-detector known as photon shot-noise. The photon shot-noise sets the limit for references [36–43]. A frequency standard whose Allan deviation [44] is limited by photon shot-noise limit can be written as [45],

$$\sigma_y^{(SN)} = \frac{1}{\nu_0}\sqrt{\frac{S_f}{2\tau}}, \tag{1}$$

where,

$$S_f = \left(\frac{g}{p}\right)^2 \frac{S_v}{2}. \tag{2}$$

τ is the averaging time, ν_0 is the clock transition frequency, g is the mixer gain, p is the error signal slope and S_v and S_f are the measured voltage and frequency noise, respectively, in the detector bandwidth. Reduction of shot-noise can be achieved by improving the error signal slope, p. In fluorescence based frequency standards p can be increased by improving collection efficiency, although this has a upper limit. The collection efficiency for this work and Lemke et al. [38] is $\sim 7 - 8\%$ of the fluoresced photons, with the currently best reported number Perrella of 15% [46] Alternatively, amplified probe light intensity can increase p, consequently, ac-Stark effects may limit long-term performance [43].

2.0.2 Intermodulation Limit

All oscillators have broadband noise, consequently, this noise bypasses filtering and demodulation in error signal generation. In continuous wave frequency modulation this is known as the intermodulation limit for the oscillator (the Dick effect for pulsed systems). The intermodulation limit sets the short-term performance for references [33, 34], restricting fractional frequency performance to 3×10^{-12} at one second. The intermodulation limit is derived in [47] and can be written as,

$$\sigma_y^{(IM)} = \frac{(S_y^{(LO)}[2f_m])^{1/2}}{2\sqrt{\tau}}, \tag{3}$$

where $S_y^{(LO)}[2f_m]$ is the laser frequency noise at twice the modulation frequency. Ahern et al. [42] noted that for multi-photon processes the frequency noise on each photon needs to be included. Consequently, the total state intermodulation limit needs to sum

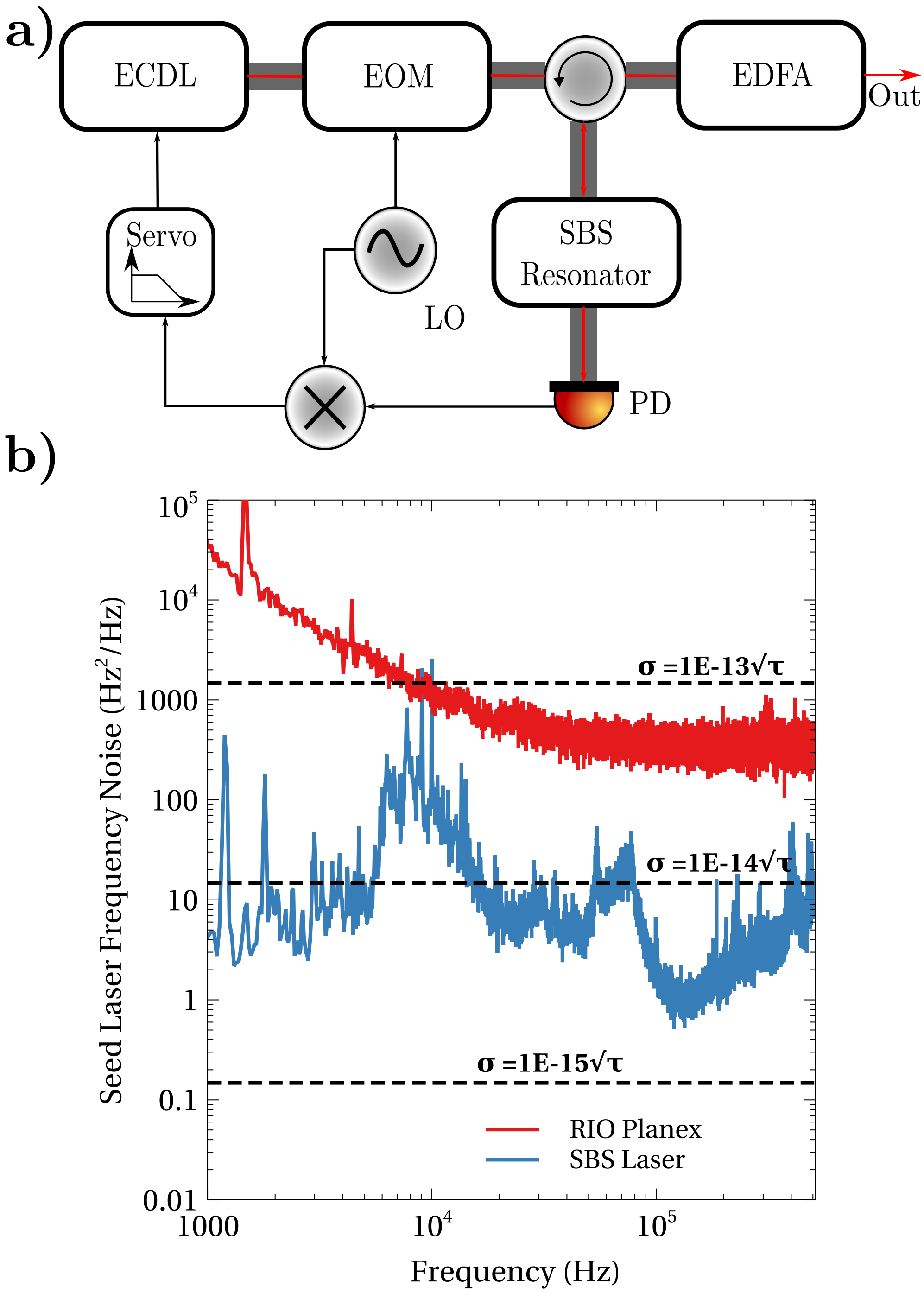

Fig. 1 (a) System diagram of the ECDL locked to an integrated silicon nitride resonator, as described in the text. The stimulated Brillouin scattering output (labeled out) is used to probe the $5S_{1/2} \rightarrow 5D_{5/2}$ two-photon transition. (b) The decrease in measured frequency noise of the SBS laser over the ECDL as measured against a stable cavity locked laser (fractional frequency $< 3 \times 10^{-15}$ at one second). Horizontal lines indicating intermodulation limited clock performance are also shown. PD-photodiode, EDFA- erbium doped fiber amplifier, EOM- electro-optic modulator, ECDL- external cavity diode laser, LO-local oscillator, SBS-stimulated Brillouin scattering.

over the frequency noise of each excitation photon, this was overlooked in Martin et al. [43]. Correlated noise from two sources (e_1 and e_2) adds as,

$$e_y = \sqrt{e_1^2 + e_2^2 + 2ce_1e_2}, \tag{4}$$

where $-1 \leq c \leq 1$ is the correlation parameter. The intermodulation limit for a degenerate two-photon excitation ($c = 1$), can now be re-written,

$$\sigma_y^{(IM)} = \frac{(S_y^{(LO)}[2f_m])^{1/2}}{\sqrt{\tau}}. \tag{5}$$

Typically, laser noise is inversely proportional to offset frequency. Consequently, the intermodulation limit can be suppressed by increasing the modulation frequency, although the atomic lifetime sets an upper limit for this noise reduction technique for florescence detection, for two-photon rubidium this upper limit is ~ 2 MHz. Ultimately, for frequency standards operating in the intermodulation limit a higher quality, narrower laser is required.

In some instances both the photon shot-noise and intermodulation limits are sufficiently small and the short-term limit is driven by environmental instabilities. This is the case in Perrella et al. [48], where clock laser alignment limited performance. Reducing the short-term limit of the two-photon Rb frequency standard requires reduction of both the intermodulation and shot-noise limits as well as careful consideration to all environmental instabilities.

3 Materials and Methods

The experimental apparatus is evolved from the system described in [38]. However, in order to suppress both intermodulation and shot-noise the experiment operates at increased optical intensities, relative to [38], while reducing laser frequency noise by stabilizing the clock laser to a stimulated Brillouin scattering (SBS) resonator [49]. The SBS laser resonator is fabricated on an ultra-low-loss silicon nitride platform [50]. The waveguide dimensions are 40 nm in thickness and 11 μm in width, designed to achieve low propagation loss and a low Brillouin lasing threshold. The radius of the resonator is 11.787 μm, ensuring the resonances match the Stokes shift [51]. The SBS laser has reduced laser phase noise in the high-frequency offset region ($<$ 100 kHz), propagation loss of 0.1 dB/m, and the loaded quality factor (Q) is 130 million at 1550 nm. These SBS lasers can reach a low lasing threshold of 14 mW and a sub-Hz fundamental linewidth [49]. Stabilizing the SBS output to the $5S_{1/2} \rightarrow 5D_{5/2}$ two-photon transition in ^{87}Rb similar to Isichenko et al. [52] will improve SBS stability at timescales greater than 1 second.

Two separate experiments with different clock lasers were performed: one utilizing a narrow 1556 nm RIO Planex external cavity diode laser (ECDL) with a measure instantaneous linewidth 1.1(15) kHz producing 20 mW of optical power, the second experiment stabilizes the same ECDL to a resonator generating SBS, see Figure 1. To

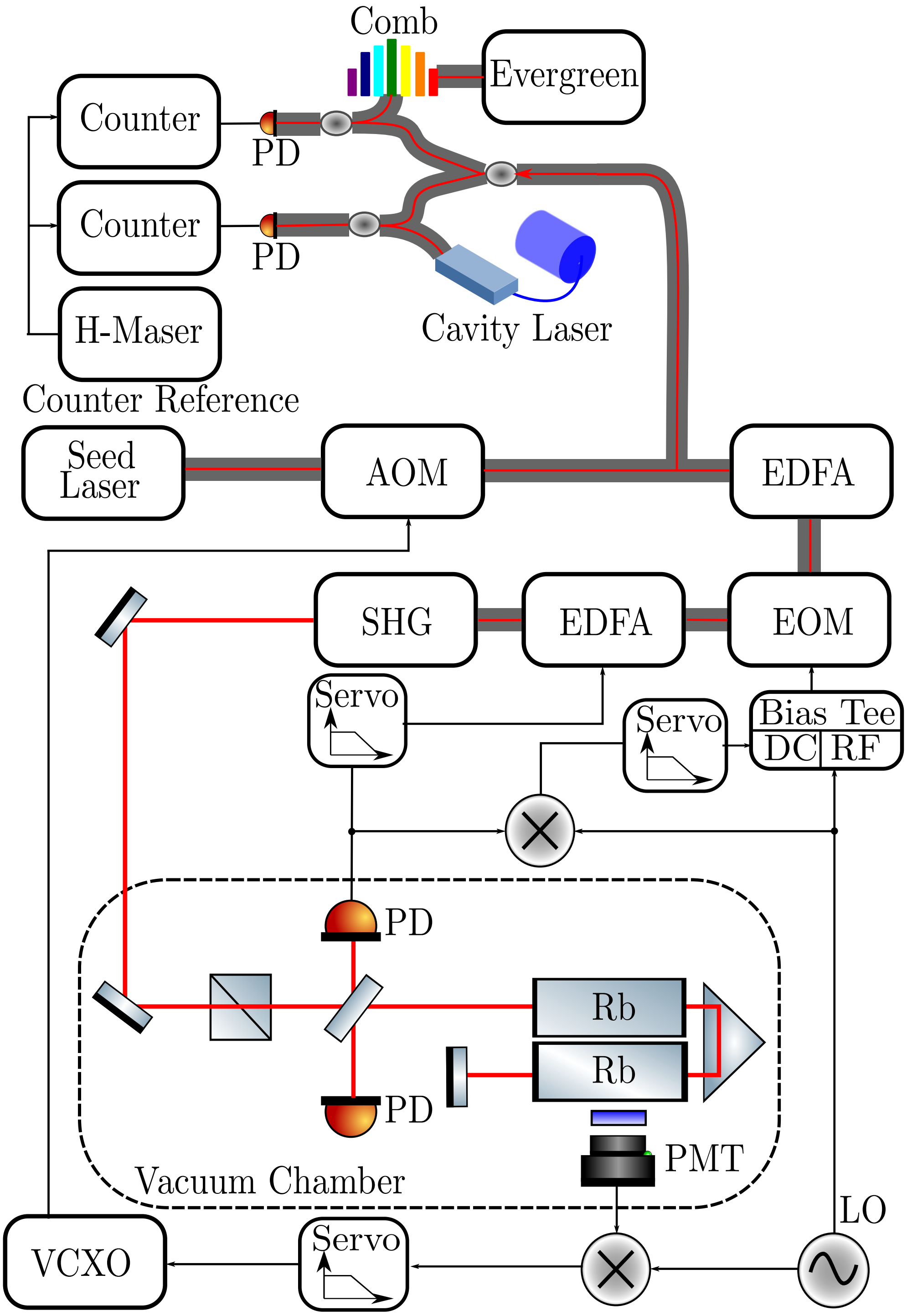

Fig. 2 System diagram of the SBS laser locked to the two-photon transition in Rb as described in the text. The clock laser is directly compared via a heterodyne with both a cavity-stabilized laser and an optical frequency comb stabilized to a molecular iodine standard labeled Evergreen in the figure. PD-photodiode, EDFA- erbium doped fiber amplifier, EOM- electro-optic modulator, LO-local oscillator, SBS-stimulated Brillouin scattering, VCXO-voltage controlled crystal oscillator, AOM -Acoustic optic modulator, SHG-second harmonic generation, PMT-Photomultiplier Tube.

produce SBS, light from the ECDL is sent through a fiber coupled waveguide electro-optical phase modulator (EOM) driven at 22 MHz to generate frequency sidebands for Pound-Drever-Hall (PDH) lock [53]. The light is then sent through a circulator to the integrated resonator, where the transmitted light is detected using a InGaAs photodiode. The counter-propagating SBS first order Stokes signal is sent back through the circulator and then to an erbium doped fiber amplifier (EDFA). After this point the laser system for the two separate experiments are identical. Figure 1 also shows the measured decrease in frequency noise of the SBS output over the ECDL, measured directly via optical heterodyne between the seed laser and a reference cavity laser with a sub-hertz linewidth, SLS-INT-1550-200-1 [54].

Figure 2 shows the experimental diagram after seed laser generation. The laser, ECDL or SBS, is sent to a fiber coupled acoustic optical modulator (AOM) frequency shifter, the actuator for atomic stabilization. At this point approximately ten percent of the optical power is sampled to be measured against a reference. The laser is sent through a pre-amplification EDFA, followed by another low RAM EOM [55, 56] modulated at 101 kHz, targeting the lowest phase noise of the SBS and ECDL. The light is sent through another EDFA and undergoes second harmonic generation (SHG) in a PPLN waveguide producing as much as 100 mW of light at 778.1 nm.

The generated 778.1 nm light is carried by optical fiber to a vacuum chamber enclosing the Rb cell apparatus. The entire free-space portion is mounted to a temperature controlled water-cooled breadboard. The light is collimated to a beam with an intensity radius ($1/e^2$) of $w_0 = 1.05(2)$ mm. The free space laser is directed through a long-pass filter to eliminate unintended third harmonic light [57], a polarizer, and a pellicle beam-splitter to sample the light for power stabilization. The beam passes through two fused silica vapor cells (length 50 mm, diameter 10 mm) connected via a 180° turning prism and enclosed in mu-metal to reduce background magnetic fields. The cells are filled with isotopically pure ^{87}Rb and heated to 100°C using low field resistive heaters. Although previous experiments used a cat's eye retro-reflector [37, 38, 58], a flat mirror was chosen to reduce pointing stability requirements on the collimator [43]. A large area PMT is mounted on top of the vapor cells behind a short-pass optical filter to collect the 420 nm fluorescence from the rubidium atoms with high efficiency.

The PMT output is demodulated with a temperature stabilized analog mixer at 101 kHz to generate the error signal. An analog servo controller with dual integrators and approximately 20 kHz bandwidth stabilizes the laser frequency by steering the shift applied by the AOM to the peak of the fluorescence signal.

InGaAs photodiodes with low capacitance (< 2 nF) in photovoltaic mode detect each reflection from the pellicle beam-splitter. Although the responsivity is lower for InGaAs than Si, the differential temperature responsivity coefficient for InGaAs is smaller than Si, making the detector less susceptible to thermal fluctuations. The detector response is amplified using a transimpedence amplifier (bandwidth > 1 MHz); the 778.1 nm laser power is stabilized to the forward beam pick-off adjusting the pump current of the final EDFA. Additionally, the signal from the photodiode is mixed with 101 kHz sinusoidal signal generating an error signal used to suppress RAM by feedback to a dc-bias across the EOM [56]. The second photodiode is used as a witness for both the power servo and RAM servo, used to measure how well these environmental instabilities are suppressed.

The stabilized 1556 nm seed light (ten percent sampled after the AOM), is then sent to be compared against two references: the SLS cavity laser and a Vector Atomic Evergreen-30 iodine frequency standard, via optical heterodyne. Each heterodyne detection was measured with a frequency counter referenced to a hydrogen maser. Since the heterodyne is generated in the optical domain, the frequency counter only requires mHz level measurement stability to measure optical frequency instabilities $< 1 \times 10^{-15}$.

4 Results

Measured clock performance can be impacted by environmental variables, reference clock performance, shot-noise and intermodulation noise. Ideally, all of the environmental impacts on the frequency standard are well understood, measured, and suppressed. However, equation 6 sums the intermodulation, shot-noise limit, and direct measurements of remaining impacts from ac-Stark ($\sigma_y^{(ac-Stark)}$), RAM ($\sigma_y^{(RAM)}$), Rb-Rb collisional $\sigma_y^{(Rb-Rb)}$, and the reference clock ($\sigma_y^{(ref)}$), yielding a prediction of clock performance from environmental effects,

$$\begin{aligned}\sigma_y(\tau)^2 &= (\sigma_y^{(IM)}(\tau))^2 + (\sigma_y^{(SN)}(\tau))^2 \\ &\quad + (\sigma_y^{(RAM)}(\tau))^2 + (\sigma_y^{(ac-Stark)}(\tau))^2 + (\sigma_y^{(Rb-Rb)}(\tau))^2 + (\sigma_y^{(ref)}(\tau))^2.\end{aligned} \tag{6}$$

To calculate ac-Stark limited performance, the rear-going photodiode measurement was calibrated converting detected voltage to optical power. This optical power measurement, free-space beam waist, and the ac-Stark transfer function found in [43] of $2.5 \times 10^{-13}/(\mathrm{mW/mm^2})$ are used to calculate $\sigma_y^{(ac-Stark)}(\tau)$. For Rb-Rb collisional limited clock performance out-of-loop temperature measurements scaled by the temperature transfer function in [58] of 1.1×10^{-12}/K are used to calculate $\sigma_y^{(Rb-Rb)}(\tau)$. Additionally, prior to clock measurement, a low frequency sinusoid was applied to the dc port of the bias tee whose output is sent to the EOM seen in Figure 2 to determine the proper scaling of detected RAM to clock frequency and calculate RAM limited clock performance, $\sigma_y^{(RAM)}(\tau)$. Finally, shot-noise limit and intermodulation limit using Equations 1, 2, and 5 with values measured and reported in Table 1 are also calculated. All of these clock limits are shown in Figure 3.

The fractional frequencies of the references were measured directly in separate experiments. The stability of the cavity locked laser was measured via optical heterodyne with two independent cavity lasers of similar performance [59] and determined to be $3.5(3) \times 10^{-15}$ at one second with a drift of 2.5(5) kHz/day driven by the laboratory environment. The cavity laser performs well in the short-term while the the Vector Atomic Evergreen-30 iodine frequency standard was used for long-term comparisons. The iodine clock was measured against the reference cavity laser using an

Table 1 Free-space laser measured parameters alongside measurements necessary to calculate the intermodulation and shot-noise limit of a given experiment.

Parameter	value
Shared values	
Atomic transition linewidth	476(13) kHz
Optical input power	58.4(3) mW
Mixer gain (g)	0.58(4)
Beam waist radius	1.05(2) mm
Amplifier Seed: RIO Planex Laser	
Instantaneous linewidth	1.10(15) kHz
Error signal slope (p)	1.0(2)μV/Hz
Voltage spectral density (S_v)	$1.0(4) \times 10^{-10}$ V^2/Hz
Power spectral density[1]	373(22)Hz^2/Hz
$\sigma_y^{(IM)}(\tau = 1\ s)$	$5.0(2) \times 10^{-14}$
$\sigma_y^{(SN)}(\tau = 1\ s)$	$7.5(20) \times 10^{-15}$
Amplifier Seed: SBS Laser	
Instantaneous linewidth	8(2)Hz
Error signal slope (p)	1.08(3) μV/Hz
Voltage spectral density (S_v)	$3.6(2) \times 10^{-11}$V^2/Hz
Power spectral density[1]	1.8(2)Hz^2/Hz
$\sigma_y^{(IM)}(\tau = 1\ s)$	$3.46(20) \times 10^{-15}$
$\sigma_y^{(SN)}(\tau = 1\ s)$	$4.2(3) \times 10^{-15}$

[1] At 202 kHz

optical heterodyne as well as compared with a second Vector Atomic Evergreen iodine standard; it's stability was determined to be $3.1(1) \times 10^{-14}/\sqrt{\tau}$ for 100 seconds with a specified drift rate of < 700 Hz/day [60].

Figure 3 shows measured clock performance when compared to two stable references. For simplicity, only the lesser of the two instabilities are shown as the measured result in Fig. 3, thereby ignoring instabilites and drifts that occur from imperfect references. Additional details of individual reference clock heterodyne measurements can be found in supplementary Figure 4. Moreover, equation 6 is used to calculate the expected clock performance given environmental measurements. This calculation is also shown in Figure 3, and is in good agreement with measured performance over short and long timescales, within a factor of four for the duration of the experiment.

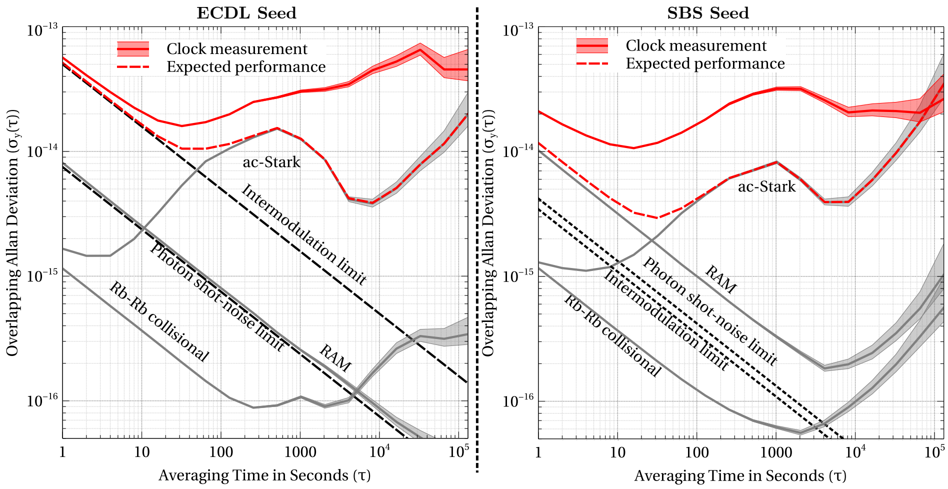

Fig. 3 Alongside the measured and expected clock performance are the measured environmental driven instabilities: Rb-Rb collisional, RAM, and ac-Stark all properly scaled to account for the impact on clock stability.

For the ECDL clock-based system, short-term instability is set by the intermodulation limit. The heterodyne measurement between the stabilized clock laser and either the iodine frequency comb or the cavity laser system yield similar results. For this clock laser both references are more stable than the two-photon clock.

For the SBS clock laser, a dramatic decrease in the intermodulation limit is predicted. Additionally, a discrepancy begins to appear between the cavity and iodine heterodynes. In this case the two-photon clock outperforms the iodine frequency standard at one second averaging times. However, neither the predicted shot-noise or intermodulation limits explain the one second instability. The RAM of the system appears to be limiting clock performance in the short term, measured performance $< 2\times$ worse then expected. Since there is still excess SNR a future experiment could be planned to demodulate using the third harmonic and further reduce the impact of RAM, at the cost of SNR [38, 61], or by leveraging more advanced RAM mitigation techniques [62].

At timescales beyond 100 seconds both clock laser choices show similar performance. The long-term stability (in this case $> 1 \times 10^5$ seconds) is limited by power instability via ac-Stark shift. This could be improved with new ac-Stark mitigation techniques [63] and using digital servos to reduce voltage setpoint drifts [38].

Mid-term performance limitation remains a bit of a mystery. The biggest disagreement between measured and expected performance occurs around 10000 seconds. Laboratory temperature was oscillating for the duration of each experiment with a period of 2000 seconds. This oscillating room temperature led to variations in thermal load on the recirculating chiller resistor and materialized as temporary disturbances in stable base-plate temperature. This is the suspected cause for the bump at this timescale of both the expected and measured performance and the disagreement between measured and expected performance. Initially, small changes in optical alignment, driven by temperature fluctuations of the free-space optical breadboard, were suspected as the cause for this mid-term mystery. Therefore, a silicon quadrant photodiode was placed at the rear-going pick-off location. Frequency stability data and environmental data were collected as the temperature set-point of the free-space optical breadboard was varied. The total observed intensity of the light appears to vary under thermal fluctuations on the quadrant photodiode a known problem with silicon detectors [64], however, the location of the centroid moved under thermal fluctuations, see the supplementary Figure 5 for further details. Small heaters were also installed around each photodiode, the Glan polarizer, the fiber collimator, and the retro-reflector. While shifts were measured while activating these heaters, no measurable frequency shifts were observed when the collimator heater was energized. The authors suspect that a combination of temperature gradients causing Rb-Rb pressure shifts, residual temperature dependent photodiode detectivity variations on the InGaAs photodiodes, and alignment ac-Stark shifts are the causes for the both mid-term instability, and the disagreement between expected and measured performance.

5 Discussion

We prioritized improvement of short-term clock stability and have demonstrated that using an SBS laser in combination with increased optical intensities can reduce the short-term instability of this two-photon transition in Rb. We were successful in increasing the short-term stability by over a magnitude over our previous reports. However, this came at the cost of increased ac-Stark shift. Additionally, we discovered that RAM eventually becomes our largest instability in the short-term. There exists methods of suppressing both RAM [38, 61, 62] and ac-Stark [63] in the literature and this frequency standard, in it's current form, would benefit from these mitigating techniques. Moreover, ovenization of the free-space optical components would yield improvement in mid-term performance and is required for operation in the field. The results obtained here will be important for the development of a deployable optical atomic clocks with high frequency stability across all timescales. Deployable optical clocks are vital component that will become essential for future communication, navigation and sensing technologies.

References

[1] Maleki, L., Prestage, J.: Applications of clocks and frequency standards: from the routine to tests of fundamental models. Metrologia **42**(3), 145 (2005) https://doi.org/10.1088/0026-1394/42/3/S15

[2] McNeff, J.G.: The global positioning system. IEEE Transactions on Microwave Theory and Techniques **50**(3), 645–652 (2002) https://doi.org/10.1109/22.989949

[3] Formichella, V., Camparo, J., Tavella, P.: Influence of the ac-stark shift on gps atomic clock timekeeping. Applied Physics Letters **110**(4), 043506 (2017) https://doi.org/10.1063/1.4975071

[4] Sinclair, L.C., Bergeron, H., Swann, W.C., Khader, I., Cossel, K.C., Cermak, M., Newbury, N.R., Deschênes, J.-D.: Femtosecond optical two-way time-frequency transfer in the presence of motion. Phys. Rev. A **99**, 023844 (2019) https://doi.org/10.1103/PhysRevA.99.023844

[5] Bergeron, H., Sinclair, L., Swann, W., Nelson, C., Deschênes, J., Baumann, E., Giorgetta, F., Coddington, I., NR, N.: Tight real-time synchronization of a microwave clock to an optical clock across a turbulent air path. Optica, 441–447 (2016) https://doi.org/10.1364/OPTICA.3.000441

[6] Deschênes, J.-D., Sinclair, L.C., Giorgetta, F.R., Swann, W.C., Baumann, E., Bergeron, H., Cermak, M., Coddington, I., Newbury, N.R.: Synchronization of distant optical clocks at the femtosecond level. Phys. Rev. X **6**, 021016 (2016) https://doi.org/10.1103/PhysRevX.6.021016

[7] Khader, I., Bergeron, H., Sinclair, L., Swann, W., Newbury, N., Deschênes, J.-D.: Time synchronization over a free-space optical communication channel. Optica (2018)

[8] Bigelow, M.S., Guidice, R., Martin, K., Metcalf, A.J., Lemke, N.: Free-space optical time transfer between an atomic frequency standard and a simple optical clock. In: 2019 Conference on Lasers and Electro-Optics (CLEO), pp. 1–2 (2019). https://doi.org/10.1364/CLEO_SI.2019.STh3G.1

[9] Olson, J., Rockmore, R., Lemke, N.D., Krzyzewski, S., Kasch, B.: Electro-optic time transfer with femtosecond stability. Applied Physics Letters **126**(11), 111103 (2025) https://doi.org/10.1063/5.0240786

[10] Holtom, J., Ma, O., Herschfelt, A., Lenz, I., Li, Y., Bliss, D.W.: Distributed coherent mesh beamforming (discobeam) for robust wireless communications. IEEE Transactions on Wireless Communications **23**(11), 15814–15828 (2024) https://doi.org/10.1109/TWC.2024.3433538

[11] Mudumbai, R., Brown Iii, D.R., Madhow, U., Poor, H.V.: Distributed transmit beamforming: challenges and recent progress. IEEE Communications Magazine **47**(2), 102–110 (2009) https://doi.org/10.1109/MCOM.2009.4785387

[12] Huntemann, N., Sanner, C., Lipphardt, B., Tamm, C., Peik, E.: Single-ion atomic clock with 3×10^{-18} systematic uncertainty. Phys. Rev. Lett. **116**, 063001 (2016) https://doi.org/10.1103/PhysRevLett.116.063001

[13] Marshall, M.C., Castillo, D.A.R., Arthur-Dworschack, W.J., Aeppli, A., Kim, K., Lee, D., Warfield, W., Hinrichs, J., Nardelli, N.V., Fortier, T.M., Ye, J., Leibrandt, D.R., Hume, D.B.: High-stability single-ion clock with 5.5×10^{-19} systematic uncertainty. Phys. Rev. Lett. **135**, 033201 (2025) https://doi.org/10.1103/hb3c-dk28

[14] Brewer, S.M., Chen, J.-S., Hankin, A.M., Clements, E.R., Chou, C.W., Wineland, D.J., Hume, D.B., Leibrandt, D.R.: ^{27}al^{+} quantum-logic clock with a systematic uncertainty below 10^{-18}. Phys. Rev. Lett. **123**, 033201 (2019) https://doi.org/10.1103/PhysRevLett.123.033201

[15] Grebing, C., Al-Masoudi, A., Dörscher, S., Häfner, S., Gerginov, V., Weyers, S., Lipphardt, B., Riehle, F., Sterr, U., Lisdat, C.: Realization of a timescale with an accurate optical lattice clock. Optica **3**(6), 563–569 (2016) https://doi.org/10.1364/OPTICA.3.000563

[16] Bothwell, T., Kedar, D., Oelker, E., Robinson, J.M., Bromley, S.L., Tew, W.L., Ye, J., Kennedy, C.J.: Jila sri optical lattice clock with uncertainty of 2.0×10^{-18}. Metrologia **56**(6), 065004 (2019) https://doi.org/10.1088/1681-7575/ab4089

[17] McGrew, W.F., Zhang, X., Fasano, R.J., Schäffer, S.A., Beloy, K., Nicolodi, D., Brown, R.C., Hinkley, N., Milani, G., Schioppo, M., Yoon, T.H., Ludlow, A.D.: Atomic clock performance enabling geodesy below the centimetre level. Nature **564**(7734), 87–90 (2018) https://doi.org/10.1038/s41586-018-0738-2

[18] Delehaye, M., Lacroûte, C.: Single-ion, transportable optical atomic clocks. Journal of Modern Optics **65**(5-6), 622–639 (2018) https://doi.org/10.1080/09500340.2018.1441917 https://doi.org/10.1080/09500340.2018.1441917

[19] Kong, D., Wang, Z.-H., Guo, F.-C., Zhang, Q., Lu, X., Wang, Y., Chang, H.: A transportable optical lattice clock at the national time service center. Chinese Physics B **29**, 070602 (2020)

[20] Takamoto, M., Ushijima, I., Ohmae, N., Yahagi, T., Kokado, K., Shinkai, H.-a., Katori, H.: Test of general relativity by a pair of transportable optical lattice clocks. Nature Photonics **14**, 411–415 (2020)

[21] Ohmae, N., Takamoto, M., Takahashi, Y., Kokubun, M., Araki, K., Hinton, A., Ushijima, I., Muramatsu, T., Furumiya, T., Sakai, Y., Moriya, N., Kamiya, N., Fujii, K., Muramatsu, R., Shiimado, T., Katori, H.: Transportable strontium optical lattice clocks operated outside laboratory at the level of 10^{-18} uncertainty. Advanced Quantum Technologies **4** (2021)

[22] Origlia, S., Pramod, M.S., Schiller, S., Singh, Y., Bongs, K., Schwarz, R., Al-Masoudi, A., Dorscher, S., Herbers, S., Hafner, S., Sterr, U., Lisdat, C.: Towards an optical clock for space: Compact, high-performance optical lattice clock based on bosonic atoms. Physical Review A (2018)

[23] Khabarova, K.Y., Kryuchkov, D., Borisenko, A.S., Zalivako, I.V., Semerikov, I., Aksenov, M.D., Sherstov, I.V., Abbasov, T., Tausenev, A.V., Kolachevsky, N.N.: Toward a new generation of compact transportable yb+ optical clocks. Symmetry **14**, 2213 (2022)

[24] Gozzelino, M., Micalizio, S., Calosso, C.E., Belfi, J., Sapia, A., Gioia, M., Levi, F.: Realization of a pulsed optically pumped rb clock with a frequency stability below 10^{-15}. Scientific Reports **13**(1), 12974 (2023) https://doi.org/10.1038/s41598-023-39942-5

[25] Ascarrunz, F.G., Dudin, Y.O., Delgado Aramburo, M.C., Ascarrunz, L.I., Savory, J., Banducci, A., Jefferts, S.R.: A portable cold 87rb atomic clock with frequency instability at one day in the 10^{-15} range. In: 2018 IEEE International Frequency Control Symposium (IFCS), pp. 1–3 (2018). https://doi.org/10.1109/FCS.2018.8597585

[26] Cole, G.D., Koller, S., Greve, C., Barwood, G.P., Deutsch, C., Gaynor, P., Ghulinyan, M., Gill, P., Hendricks, R., Hill, I., Kundermann, S., Goff, R.L., Lecomte, S., Meier, C., Pepponi, G., Schilt, S., Stenzel, C., Sütterlin, R., Voss, K., Zhukov, A.: Towards space-deployable laser stabilization systems based on vibration-insensitive cubic cavities with crystalline coatings. Opt. Express **32**(4), 5380–5396 (2024) https://doi.org/10.1364/OE.506833

[27] Kelleher, M.L., McLemore, C.A., Lee, D., Davila-Rodriguez, J., Diddams, S.A., Quinlan, F.: Compact, portable, thermal-noise-limited optical cavity with low acceleration sensitivity. Opt. Express **31**(7), 11954–11965 (2023) https://doi.org/10.1364/OE.486087

[28] Hilton, A.P., Offer, R.F., Klantsataya, E., Scholten, S.K., Bourbeau Hébert, N., Billington, C.J., Locke, C., Perrella, C., Nelligan, M., Allison, J.W., White, B., Ahern, E., Martin, K.W., Beard, R., Elgin, J.D., Sparkes, B.M., Luiten, A.N.: Demonstration of a mobile optical clock ensemble at sea. Nature Communications **16**(1), 6063 (2025) https://doi.org/10.1038/s41467-025-61140-2

[29] Roslund, J.D., Cingöz, A., Lunden, W.D., Partridge, G.B., Kowligy, A.S., Roller, F., Sheredy, D.B., Skulason, G.E., Song, J.P., Abo-Shaeer, J.R., Boyd, M.M.: Optical clocks at sea. Nature **628**(8009), 736–740 (2024) https://doi.org/10.1038/s41586-024-07225-2

[30] Martin, M.J., Foreman, S.M., Schibli, T.R., Ye, J.: Testing ultrafast mode-locking at microhertz relative optical linewidth. Optics Express **17**(2), 558–568 (2009)

[31] Obaze-Adeleke, A.C., Semon, B., Bandi, T.N.: A comprehensive review of rubidium two-photon vapor cell optical clock: Long-term performance limitations and potential improvements. Photonics **12**(5) (2025) https://doi.org/10.3390/photonics12050513

[32] Erickson, S.E., Tooley, D.P., Weerasinghe, K., Zhu, X., Chavez-Pirson, A., Jones, R.J.: Atomic frequency standard based on direct frequency comb spectroscopy. Opt. Lett. **49**(19), 5340–5343 (2024) https://doi.org/10.1364/OL.531600

[33] Maurice, V., Newman, Z.L., Dickerson, S., Rivers, M., Hsiao, J., Greene, P.,

Mescher, M., Kitching, J., Hummon, M.T., Johnson, C.: Miniaturized optical frequency reference for next-generation portable optical clocks. Opt. Express **28**(17), 24708–24720 (2020) https://doi.org/10.1364/OE.396296

[34] Newman, Z.L., Maurice, V., Drake, T., Stone, J.R., Briles, T.C., Spencer, D.T., Fredrick, C., Li, Q., Westly, D., Ilic, B.R., Shen, B., Suh, M.-G., Yang, K.Y., Johnson, C., Johnson, D.M.S., Hollberg, L., Vahala, K.J., Srinivasan, K., Diddams, S.A., Kitching, J., Papp, S.B., Hummon, M.T.: Architecture for the photonic integration of an optical atomic clock. Optica **6**(5), 680–685 (2019) https://doi.org/10.1364/OPTICA.6.000680

[35] Callejo, M., Mursa, A., Vicarini, R., Klinger, E., Tanguy, Q., Millo, J., Passilly, N., Boudot, R.: Short-term stability of a microcell optical reference based on the rb atom two-photon transition at 778 nm. J. Opt. Soc. Am. B **42**(1), 151–159 (2025) https://doi.org/10.1364/JOSAB.533904

[36] Li, D., Liu, K., Zhao, L., Kang, S.: A frequency shift compensation method for light shift and vapor-cell temperature shift in atomic clocks (2024). https://arxiv.org/abs/2405.14281

[37] Beard, R., Martin, K.W., Elgin, J.D., Kasch, B.L., Krzyzewski, S.P.: Two-photon rubidium clock detecting 776 nm fluorescence. Opt. Express **32**(5), 7417–7425 (2024) https://doi.org/10.1364/OE.513974

[38] Lemke, N.D., Martin, K.W., Beard, R., Stuhl, B.K., Metcalf, A.J., Elgin, J.D.: Measurement of optical rubidium clock frequency spanning 65 days. Sensors **22**(5) (2022) https://doi.org/10.3390/s22051982

[39] Poulin, M., Latrasse, C., Touahri, D., Têtu, M.: Frequency stability of an optical frequency standard at 192.6 thz based on a two-photon transition of rubidium atoms. Optics Communications **207**(1), 233–242 (2002) https://doi.org/10.1016/S0030-4018(02)01354-8

[40] Gerginov, V., Beloy, K.: Two-photon optical frequency reference with active ac stark shift cancellation. Phys. Rev. Appl. **10**, 014031 (2018) https://doi.org/10.1103/PhysRevApplied.10.014031

[41] Perrella, C., Light, P.S., Anstie, J.D., Baynes, F.N., White, R.T., Luiten, A.N.: Dichroic two-photon rubidium frequency standard. Phys. Rev. Appl. **12**, 054063 (2019) https://doi.org/10.1103/PhysRevApplied.12.054063

[42] Ahern, E.J., Scholten, S.K., Locke, C., Hébert, N.B., White, B., Luiten, A.N., Perrella, C.: Tailoring the stability of a two-color, two-photon rubidium frequency standard. Phys. Rev. Appl. **23**, 044025 (2025) https://doi.org/10.1103/PhysRevApplied.23.044025

[43] Martin, K.W., Stuhl, B., Eugenio, J., Safronova, M.S., Phelps, G., Burke, J.H.,

Lemke, N.D.: Frequency shifts due to stark effects on a rubidium two-photon transition. Phys. Rev. A **100**, 023417 (2019) https://doi.org/10.1103/PhysRevA.100.023417

[44] Allan, D.W.: Statistics of atomic frequency standards. Proceedings of the IEEE **54**(2), 221–230 (1966) https://doi.org/10.1109/PROC.1966.4634

[45] Hilico, L., Felder, R., Touahri, D., Acef, O., Clairon, A., Biraben, F.: Metrological features of the rubidium two-photon standards of the bnm-lptf and kastler brossel laboratories. Eur. Phys. J. AP **4**(2), 219–225 (1998) https://doi.org/10.1051/epjap:1998263

[46] Perrella, C.: Demonstration of a two-photon atomic clock with light shift suppression using two-colour magic wavelengths. Technical Report AFRL-AFOSR-JP-TR-2022-0021, The University of Adelaide, Adelaide, AUS (2022). https://apps.dtic.mil/sti/trecms/pdf/AD1169804.pdf

[47] Audoin, C., Candelier, V., Diamarcq, N.: A limit to the frequency stability of passive frequency standards due to an intermodulation effect. IEEE Transactions on Instrumentation and Measurement **40**(2), 121–125 (1991) https://doi.org/10.1109/TIM.1990.1032896

[48] Perrella, C., Light, P.S., Anstie, J.D., Baynes, F.N., Benabid, F., Luiten, A.N.: Two-color rubidium fiber frequency standard. Opt. Lett. **38**(12), 2122–2124 (2013) https://doi.org/10.1364/OL.38.002122

[49] Gundavarapu, S., Brodnik, G.M., Puckett, M., Huffman, T., Bose, D., Behunin, R., Wu, J., Qiu, T., Pinho, C., Chauhan, N., Nohava, J., Rakich, P.T., Nelson, K.D., Salit, M., Blumenthal, D.J.: Sub-hertz fundamental linewidth photonic integrated brillouin laser. Nature Photonics **13**(1), 60 (2019) https://doi.org/10.1038/s41566-018-0313-2

[50] Blumenthal, D.J., Heideman, R., Geuzebroek, D., Leinse, A., Roeloffzen, C.: Silicon nitride in silicon photonics. Proceedings of the IEEE **106**(12), 2209–2231 (2018) https://doi.org/10.1109/JPROC.2018.2861576

[51] Puckett, M.W., Liu, K., Chauhan, Q. Nitesh ans Zhao, Jin, N., Cheng, H., Wu, J., Behunin, R.O., Rakich, P.T., Nelson, K.D., Blumenthal, D.J.: 422 million intrinsic quality factor planar integrated all-waveguide resonator with sub-mhz linewidth. Nature Communications **12**(1), 934 (2021) https://doi.org/10.1038/s41467-021-21205-4

[52] Isichenko, A., Kortyna, A., Chauhan, N., Wang, J., Harrington, M.W., Olson, J., Blumenthal, D.J.: Tunable 778 nm integrated brillouin laser probe for a rubidium two-photon optical atomic clock. 2024 Conference on Lasers and Electro-Optics (CLEO) (2024)

[53] Drever, R.W.P., Hall, J.L., Kowalski, F.V., Hough, J., Ford, G.M., Munley, A.J., Ward, H.: Laser phase and frequency stabilization using an optical-resonator. Applied Physics B-Photophysics and Laser Chemistry **31**(2), 97–105 (1983)

[54] Stable Laser Systems: Hz-Level Rack Mounter Laser System. (2025). Stable Laser Systems. Date accessed: 2025-12-12. https://stablelasers.com/wp-content/uploads/2024/09/SLS_1550-200-1-SpecSheet-9.24-Digital.pdf

[55] Martin, K.W.: Compact Optical Frequency Standards for Future Applications Beyond the Laboratory (2019). https://digitalrepository.unm.edu/phyc_etds/210

[56] Zhang, W., Martin, M.J., Benko, C., Hall, J.L., Ye, J., Hagemann, C., Legero, T., Sterr, U., Riehle, F., Cole, G.D., Aspelmeyer, M.: Reduction of residual amplitude modulation to 1×10^{-6} for frequency modulation and laser stabilization. Opt. Lett. **39**(7), 1980–1983 (2014) https://doi.org/10.1364/OL.39.001980

[57] Zhang, L., Wu, X., Hao, Z., Ma, R., Gao, F., Bo, F., Zhang, G., Xu, J.: Second-harmonic and cascaded third-harmonic generation in generalized quasiperiodic poled lithium niobate waveguides. Opt. Lett. **48**(7), 1906–1909 (2023) https://doi.org/10.1364/OL.483431

[58] Martin, K.W., Phelps, G., Lemke, N.D., Bigelow, M.S., Stuhl, B., Wojcik, M., Holt, M., Coddington, I., Bishop, M.W., Burke, J.H.: Compact optical atomic clock based on a two-photon transition in rubidium. Phys. Rev. Appl. **9**, 014019 (2018) https://doi.org/10.1103/PhysRevApplied.9.014019

[59] Gray, J.E., Allan, D.W.: A method for estimating the frequency stability of an individual oscillator. In: 28th Annual Symposium on Frequency Control, pp. 243–246 (1974). https://doi.org/10.1109/FREQ.1974.200027

[60] Vector Atomic: Evergreen-30. (2025). Vector Atomic. Date accessed: 2025-12-12. https://vectoratomic.com/eg30-advanced-release

[61] Burck, F., Lopez, O.: Correction of the distortion in frequency modulation spectroscopy. Measurement Science and Technology **15**(7), 1327 (2004) https://doi.org/10.1088/0957-0233/15/7/015

[62] Nguyen, T.N., Schibli, T.R.: Field-programmable gate array-based residual amplitude modulation suppression and control for compact atomic clocks. Review of Scientific Instruments **95**(2), 023001 (2024) https://doi.org/10.1063/5.0185763

[63] Andeweg, Y., Kitching, J., Hummon, M.T.: Active compensation of the AC Stark shift in a two-photon rubidium optical frequency reference using power modulation (2025). https://arxiv.org/abs/2511.19702

[64] Ferri, A., Acerbi, F., Gola, A., Paternoster, G., Piemonte, C., Zorzi, N.: A comprehensive study of temperature stability of silicon photomultiplier. Journal of

Instrumentation **9**(06), 06018 (2014) https://doi.org/10.1088/1748-0221/9/06/P06018

Acknowledgments

Any mention of commercial products within this article is for information only; it does not imply recommendation or endorsement by the Department of the Air Force, the Department of War, or the U.S. Government. Approved for public release, distribution is unlimited. Public Affairs release approval # AFRL20260505 The views expressed are those of the authors and do not reflect the official policy or position of the Department of the Air Force, the Department of War, or the U.S. Government.

Author Contributions

K.W.M., K.C, S.K, and S.E.E. and R.B. designed the experiment. K.W.M. took and analyzed the data. K.W.M. write the first draft. A.I., D.J.B. and K.L. designed and developed the SBS resonator. All authors worked on revisions. K.C, S.K, and S.E.E. provided supervision.

Funding

This work was supported in part by the Air Force Research Labs and COSMAIC under award FA9453-20-2-001 and sub-award 282109-873R.

Data availability

Data underlying the results presented here can be provided from the authors upon reasonable request.

Ethics declarations

Competing interests

The authors declare no competing interests.

Supplementary information

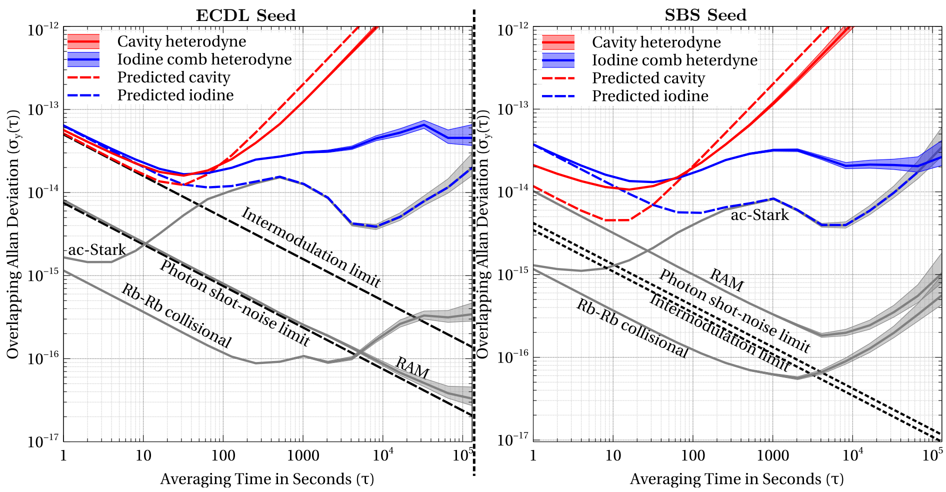

Fig. 4 Solid blue line shows the measured heterodyne between the iodine comb and the two-photon clock, while the dashed blue line show expected performance of this heterodyne including expected reference instabilities and drifts. Solid red line shows the measured heterodyne between the cavity laser and the two-photon clock, while the dashed red line show expected performance of this heterodyne including expected reference instabilities and drifts. Alongside the measured and expected clock performance are the measured environmental driven instabilities: Rb-Rb collisional, RAM, and ac-Stark properly scaled to account for their impact on clock shift

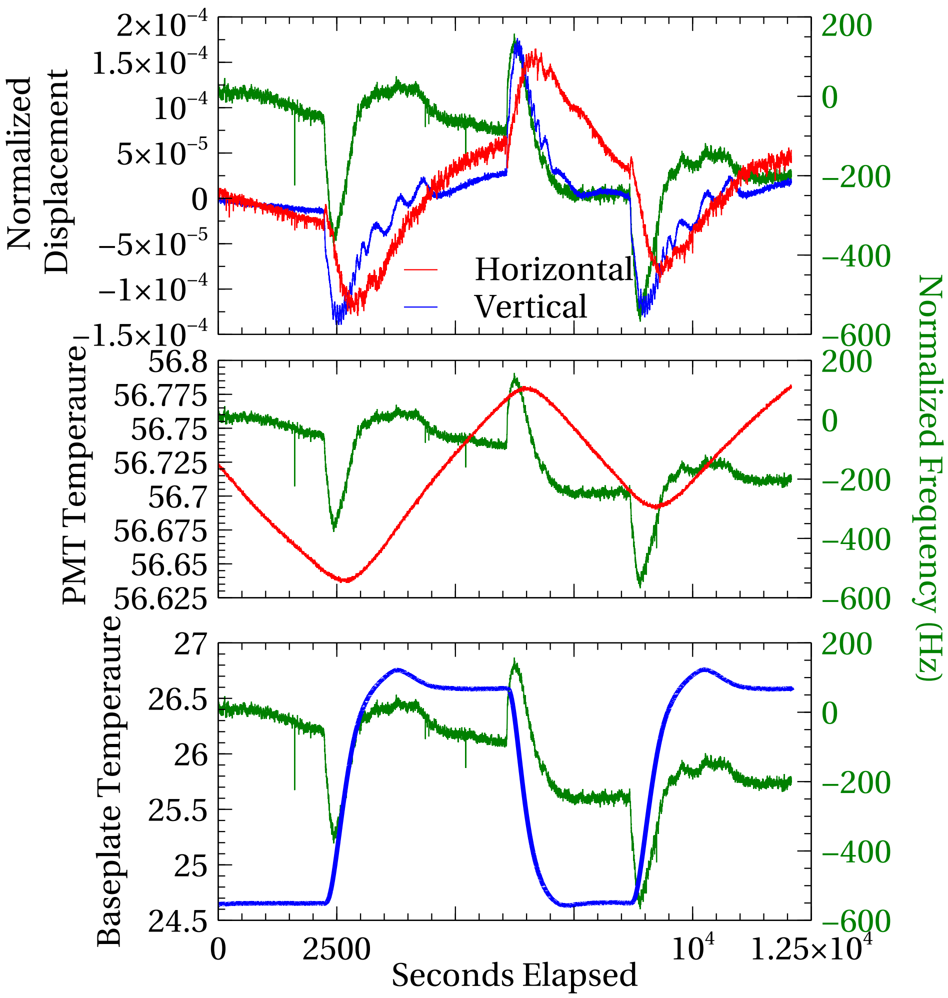

Fig. 5 The top graph shows the measured vertical (blue) and horizontal (red) alignment changes as the base plate temperature is varied as well as the frequency shifts (green). The middle graph shows the PMT temperature change (red) and frequency change (green) and the bottom graph shows the baseplate temperature change (blue) along with frequency shifts (green).